ROTORCRAFT STRUCTURAL FAILURE RISK COMPUTATIONS UNDER MULTIAXIAL VARIABLE LOADING

Dr. Suresh Moon[1] and Nam Phan[2]

[1]Chief Engineer, Air Vehicle Engineering, L-3 Communications, Lexington Park MD
[2]Branch Head, Rotary Wing Branch, Structures Division, NAVAIR, Patuxent River, MD

Abstract

Rotorcraft composite rotor hub structures are made of flexible beams to balance the centrifugal forces at the hub center and to carry shear and bending moments. One end of the composite cuff/sleeve is attached to the hub and the other end is connected to the composite rotor blade enabling changes to the blade pitch. This results in the cuff being subjected to axial, shear, torsion and bending moments (flapwise and chordwise). The sleeve is constructed as a three cell wing box structure with composite material tape and fiber placement in different orientations. This construction is difficult to manufacture consistently and as a result the rotorcraft cuff failed in static testing due to delamination and subsequent buckling at loads slightly less than 1.5 factors of safety requirements. Therefore, it is necessary to establish a relationship between the percentile strength and risk and to determine the cuff failure risk for flight qualification and operational flight tests. An approach has been formulated to compute failure risk in a flight under multiaxial variable loading. The Weibull and Normal distributions were fitted to full scale blade cuff static tests failure data, measured flight loads and measured usages from 50 aircraft. The reduction in static strength to μ-2σ value resulted in a probability of cuff failure to be 1.14×10^{-7} with Normal distribution and 8.33×10^{-9} with Weibull. Furthermore, if flapwise and chordwise loads are considered to be an independent Normal multivariable the Probability of Failure (PoF) decreases to 2.7×10^{-9} per flight. Restricting the dive speed and load factor can reduce the PoF even further. This approach helps to calculate risk and to continue rotorcraft development and flight testing.

1. INTRODUCTION

The composite bearingless rotor hub development was initiated in early 1970. Aerospatiale, France developed a start flex head for AS350/Ecuril in 1972. Aerospatiale also used the same rotor technology on SA365 Dauphin/HH-65. Since then, extensive research has improved bearingless rotor head technology, Reference 1-2. The bearingless rotor hub requires flap, lead-lag and feathering hinges be incorporated in structures as virtual hinges. These virtual/effective hinges provide the required deflection and rotations. However, the forces and moments are not completely relieved at the effective hinges, only the magnitudes are reduced significantly. The most desirable rotor hub sequence is flap hinge, lead-lag, and feathering in order to achieve optimum dynamic, stability and control characteristics and avoid aero-elastic instabilities. The deflections, rotations, and load carrying capabilities determine the hub construction. Bell helicopter initiated their bearingless rotor hub development in early 1970, Reference 3. Improvements were made in bearing rotor hub technology by Bell with respect to flapping flexure, feathering and blade/cuff/yoke attachment. The yoke was modified to incorporate low flapping hinge

offset, adequate flapping and feathering to cover a wide gross weight (g.w.) and center of gravity (c.g.) travel range. To change the blade pitch, the long structure called a torque tube/cuff, is introduced between the rotor hub and the rotor blade. The cuff construction is difficult to manufacture consistently and as a result the rotorcraft cuff failed in static test due to delamination and subsequent buckling at loads slightly less than 1.5 factors of safety requirements. Therefore, it is necessary to establish a relationship between the percentile strength reduction and risk and to determine the cuff failure risk for flight qualification and operational flight tests.

2. ROTOR HUB STRUCTURE

The detailed description of H-1 rotor hub assembly is provided in Reference 4 According to this reference, "the hub assembly as shown in Figure 1, consists of two identically stacked composite yokes, fluid-elastic dampers, elastomeric shear restraint, and pitch change adapters with integral pitch horns, composite cuffs, drive bushings, drive plate, and flapping stops". The main rotor cuff is described in Reference 4 as follows: "Pitch change or feathering motion is transmitted from pitch links to the blades through pitch change adapters and torsionally stiff composite assemblies. The cuff has an elliptical cross section to minimize drag and employs a three cell construction for ballistic tolerance. The cuffs are made primarily from fiberglass/epoxy with unidirectional carbon epoxy tape in the leading and trailing edges to provide the required stiffness", Figure 2.

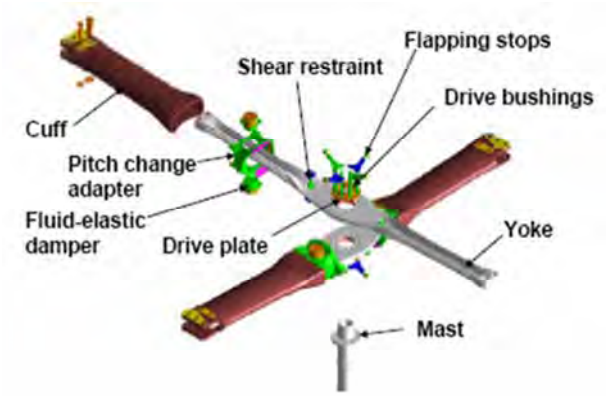

Figure 1: Main rotor hub assembly, Reference 4.

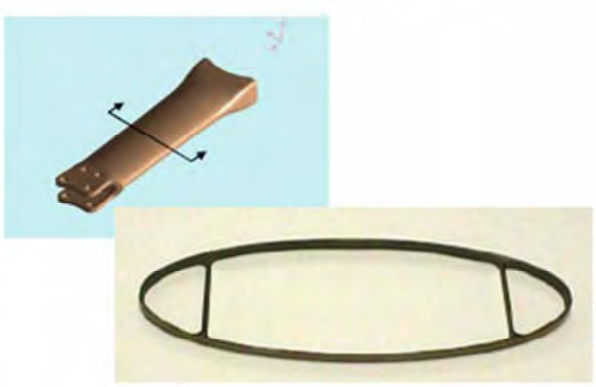

Figure 2: Main rotor cuff three-cell construction, Reference 4.

3. STRENGTH VARIATION

The cuff is a rotating cantilever beam that transfers Centrifugal Force (CF) from blade to yoke at outboard ends and carries flap/beamwise (Mx), chordwise (Mz) moments and torsion (T). To demonstrate structural integrity of the rotor blade cuff, seven full scale cuffs were tested in test fixtures at Room Temperature Dry (RTD) conditions as shown in Figure 3. Only one cuff was tested in a Hot Wet (HWET) condition. The loads applied were CF, T, Mx and Mz. The expected Mx to Mz ratio of 0.216 was maintained throughout the test. The Mx moment produced tensile stresses on the lower surface and compression at the

top surface of the cuff. Whereas the Mz moment created tensile stresses at the cuff leading edge spar and compressive stresses at the cuff rear spar of the three cell cuff structure as shown in Figure 2. Additionally, shear stresses are created in cuffs due to torsion. The rear spar top corner was subjected to maximum compressive stresses whereas the front spar lower surface was subjected to maximum tensile stresses. The compressive strain variation with Mx and Mz moments, depicted in Figure 4**,** clearly show linear variation up to the 90th percentile of moment and change in slope after the 90th percentile of moment. The change in slope is a clear indication of buckling initiation in the composite material laminate. The delaminations are initiated at the bond line between the torque tube and ballistic chambers. The delamination grows as the moment increases from 90th to 100th percentile. The delamination growth leads to failure of the ballistic chambers that subsequently result in the failure of the torque tube/cuff, Figure 3.

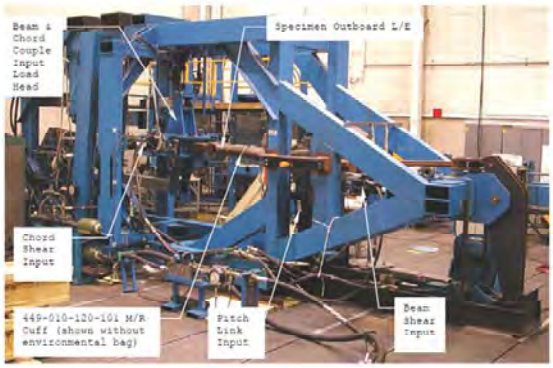

Figure 3: Cuff test setup, Reference 4.

Figure 4: Compressive strain variation with applied moments.

The seven blade cuff Mx and My failure moments (strengths) at RTD and the one cuff failure moment in HWET conditions are indicated in Figure 5. The HWET condition cuff strength variation is created using the RTD static strength data and HWET condition knock down factor of 0.67. The knock down factor was obtained from available coupon static strength data on RTD and HWET testing documented in Reference 5. The CF and torsion loads on the cuff are almost constant, thus the cuff strength depends on the magnitude of the applied Mx and Mz moments. For the PoF computations with interference theory it is necessary to model strength variation using statistical probability distributions such as Normal, Weibull, etc. These distributions can of single variable or multivariable. In the first approach single variable Normal and Weibull distributions were created with resultant moment (Mr) obtained by combining the magnitudes of Mx and Mz by expression, Mr = sqrt (Mx^2+Mz^2). In the second approach, Mx and Mz are considered multivariable variables to create Normal joint probability distributions and Weibull joint probability distribution to compute PoF.

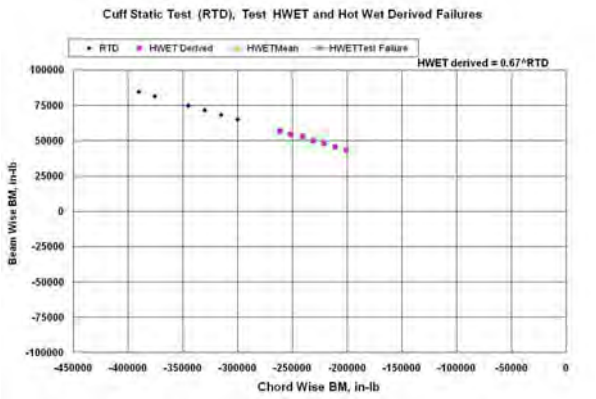

Figure 5: The fatigue test cuff failure moments.

3.1 Single variable strength distribution

The single variable Normal distribution Probability Density Function (PDF) is given by the following expression:

$$P(y) = 1/\sigma_y \sqrt{2\pi} \exp\left[-1/2 \left(\left(y - \mu_y \right)/ \sigma_y \right)^2 \right] dy$$

The cuff static component strength tests in HWET condition are used to derive, mean strength (μ) and standard deviation (σ). Further with the help of μ and σ Normal Cumulative Probability Distribution (CPD) is computed as displayed in Figure 6.

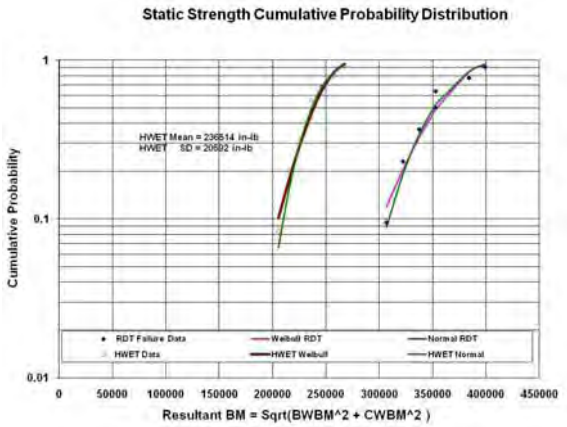

Figure 6: Static strength cumulative probability distribution.

The single variable Weibull distribution PDF is as follows, Reference 6:

$$f(y,\beta) = \frac{\beta}{(\eta)}\left(\frac{y}{\eta}\right)^{\beta-1} \exp\left[-\left(\frac{y}{\eta}\right)^{\beta}\right]$$

Where:

y = Variable
β = Weibull shape parameter
η = Weibull scale parameter

The Weibull CPD distribution is given by:

$$F(y,\beta) = 1 - \exp\left[-\left(\frac{y}{\eta}\right)^{\beta}\right]$$

The Weibull distribution parameters β and η were evaluated using least square and maximum likelihood methods. The values estimated with both approaches do not differ significantly, Table 1. However the parameters values derived by least square method have excellent correlation coefficient and are used for further analyses. The CPD of strength in RDT and HWET condition for Weibull distribution is displayed in Figure 6.

Table1: Strength Weibull and Normal Distribution Parameters

	Strength Weibull Distribution						Strength Normal Distribution	
	Least Square Method			Maximum Likelihood Method			Maximum Likelihood Method	
	ή	β	r	ή	β		μ	σ
Mz	239905	12.642	0.977	239835	13.666		231128	20113
Mx	52104	12.438	0.977	52093	13.710		50185	4426
Mr	245487	12.626	0.977	245426	13.670		236514	20592

4. USAGE VARIATIONS

The Structural Data Recording Set (SDRS) was installed on AH-1W aircraft for individual dynamic component tracking as explained in **Reference 7**. Sixty aircraft were equipped with recorders and a total of 6,000 flight hours' data was recorded over a period of almost five years from 50 aircraft. The analysis revealed significant variation in usage from helicopter to helicopter, Figures 7. The details of usage variations in each regime and their statistical modeling are discussed in References 8 and 9. For usage spectrum development, 300 recorded regimes were condensed to 74 design spectrum regimes, as indicated in Table 2. A 100-hour usage spectrum was created for 45 individual aircraft with recorded flight hours greater than 100. The individual spectra were used to create fleet average spectra indicated in, Tables 2. The step by step rotorcraft usage spectrum development using the recorded data is documented in Reference 10. The statistical parameters (μ, σ, coefficient of variation, maximum, and minimum) of each regime in the usage spectrum were computed. The damaging status of each regime was also identified using 53 life-limited components damage matrices. This information was used to create a conservative usage spectrum (μ+3σ), shown in Table 2. The spectrum created for AH-1W was provided as a specification usage spectrum to develop the four bladed composite rotor hub and rotor blade rotorcraft AH-1Z. Thus the percent time in average and (μ + 3σ) usage spectrum were converted into rotor cycles to obtain the frequency of Mx and Mz loading in each regime as shown Figure 8.

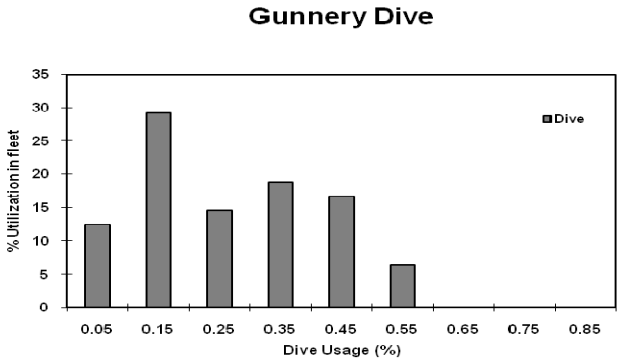

Figure 7: The regime usage variation.

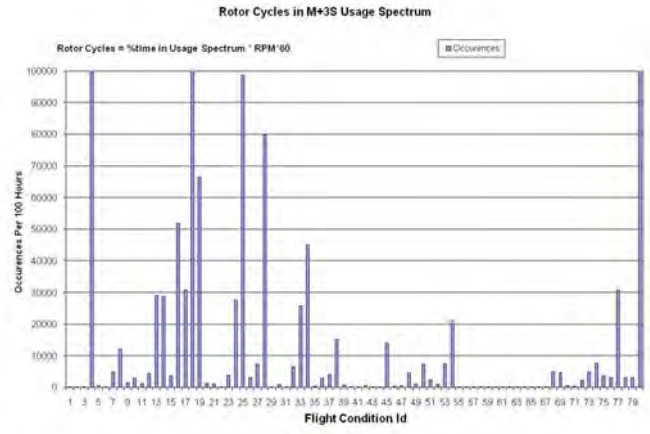

Figure 8: Rotor cycles for all flight conditions in μ+3σ usage spectrum.

Table 2: Usage Spectrum

Design Spec No.	Weight Classs	Description	Design Spect. %	Mean % Spect. %	σ	Prop. Spect.
1	Med	Normal Start	0.500	0.000	0.000	0.000
3	Med	IGE, Normal Takeoff	0.000	0.000	0.000	0.000
4	Med	IGE, Jump Takeoff	0.000	0.000	0.000	0.000
5	Med	IGE, Hover_Steady	1.770	6.855	4.814	5.675
6	Med	IGE, Hover Left Turn	0.100	0.015	0.015	0.013
7	Med	IGE, Hover Right Turn	0.100	0.007	0.011	0.006
11	Med	IGE, Sideward Flight _Left	0.250	0.132	0.512	0.109
12	Med	IGE, Sideward Flight _Right	0.250	1.128	1.683	0.273
14	Med	IGE, Normal Acceleration	0.500	0.038	0.052	0.032
15	Med	IGE, Deceleration_Normal	0.500	0.078	0.079	0.065
16	Med	IGE, Deceleration_Quick Stop	0.100	0.036	0.023	0.030
17	Med	IGE, Normal Landing	0.000	0.120	0.104	0.099
18	Med	Fwd. Level Flight -0.5VH, 311 RPM	1.500	0.790	1.072	0.655
19	Med	Fwd. Level Flight -0.6VH, 311 RPM	2.500	0.782	0.747	0.648
20	Med	Fwd. Level Flight -0.7VH, 311 RPM	3.500	1.100	1.064	0.083
21	Med	Fwd. Level Flight -0.8VH, 311 RPM	9.450	1.407	1.160	1.166
22	Med	Fwd. Level Flight -0.9VH, 311 RPM	3.500	1.837	1.360	0.693
23	Med	Fwd. Level Flight -1.0VH, 311 RPM	2.500	14.840	6.755	12.295
24	Med	OGE, Full Power Climb - Twin Eng.	2.100	1.809	1.527	1.499
25	Med	OGE, Full Power Climb - Single Eng.	0.085	0.036	0.125	0.030
26	Med	OGE, Max Rate Acceleration	0.875	0.006	0.008	0.024
27	Med	OGE, Max Rate Deceleration	0.790	0.000	0.000	0.000
28	Med	OGE, Standard Turn - Left 0.5VH	0.220	0.102	0.102	0.085
29	Med	OGE, Standard Turn - Left 0.7VH	0.875	0.211	0.180	0.623
30	Med	OGE, Standard Turn - Left 0.9VH	0.655	1.085	0.533	2.223
31	Med	OGE, Standard Turn - Right 0.5VH	0.220	0.086	0.077	0.071
32	Med	OGE, Standard Turn - Right 0.7VH	0.875	0.199	0.167	0.165
33	Med	OGE, Standard Turn - Right 0.9VH	0.650	0.926	0.415	1.800
34	Med	OGE, 0.9VH Cont Rev - F/A	0.035	0.001	0.001	0.003
35	Med	OGE, 0.9VH Cont Rev - Lateral	0.035	0.006	0.007	0.021
36	Med	OGE, 0.9VH Cont Rev - Pedal	0.035	0.002	0.003	0.002
37	Med	OGE, Sideslip - Left	0.110	0.177	1.223	0.147
38	Med	OGE, Sideslip - Right	0.110	0.700	1.613	0.580
39	Med	OGE, Part Pwr Des - Twin Eng	1.000	1.227	0.792	1.016
40	Med	OGE, Part Pwr Des - Single Eng	0.110	0.008	0.009	0.007
41	Med	ATTACK, Gun Dives - Pt Target to 0.8VL	0.845	0.079	0.064	0.066
42	Med	ATTACK, Gun Dives - Pt Target to 0.9VL	0.420	0.021	0.029	0.090
43	Med	ATTACK, Gun Dives - Pt Target to VL	0.130	0.040	0.124	0.342
47	Med	ATTACK, Pull-Ups - To Left, 0.8VL	0.415	0.005	0.006	0.017
48	Med	ATTACK, Pull-Ups - To Left, 0.9VL	0.210	0.000	0.001	0.002
49	Med	ATTACK, Pull-Ups - To Left, VL	0.070	0.000	0.001	0.001
56	Med	ATTACK, Gun Turns - Left, 0.5VH	0.090	0.009	0.039	0.105
57	Med	ATTACK, Gun Turns - Left, 0.7VH	0.230	0.005	0.008	0.025
58	Med	ATTACK, Gun Turns - Left, 0.9VH	0.325	0.067	0.045	0.167
59	Med	ATTACK, Gun Turns - Right, 0.5VH	0.090	0.007	0.019	0.054
60	Med	ATTACK, Gun Turns - Right, 0.7VH	0.230	0.004	0.007	0.020
61	Med	ATTACK, Gun Turns - Right, 0.9VH	0.325	0.055	0.050	0.171
62	Med	ATTACK, 0.8VH S-Turn	0.850	0.170	0.136	0.478
64	Med	POWER TRANS, Twin-Single, 0.9VH	0.085	0.000	0.000	0.000
65	Med	POWER TRANS, Single-Twin	0.175	0.000	0.000	0.000
66	Med	POWER TRANS, Twin-Auto, 0.7VH	0.600	0.000	0.000	0.000
67	Med	POWER TRANS, Twin-Auto, 0.9VH	0.600	0.000	0.000	0.000
68	Med	POWER TRANS, Single-Auto, 0.5VH	0.300	0.000	0.000	0.000
70	Med	Power Recovery, Auto-Twin	1.200	0.000	0.000	0.000
71	Med	Power Recovery, Auto-Single	0.600	0.000	0.000	0.000
72	Med	AUTOROTATION, Stabilized, 60 kts.	0.150	0.005	0.017	0.004
73	Med	AUTOROTATION, Stabilized, 80 kts.	0.500	0.002	0.004	0.002
74	Med	AUTOROTATION, Stabilized, VL	0.150	0.000	0.001	0.000
75	Med	AUTOROTATION, Auto Turns, Left	0.100	0.000	0.001	0.000
76	Med	AUTOROTATION, Auto Turns, Right	0.100	0.000	0.001	0.001
77	Med	AUTOROTATION, Full Auto Landing	0.100	0.000	0.000	0.000
80	Med	ACM, HVH, High Yo-Yo	0.000	0.021	0.020	0.113
81	Med	ACM, HVH, Low Yo-Yo	0.000	0.020	0.025	0.108
83	Med	ACM, HVH, Pass, Level Turn Left - Moderat	0.000	0.001	0.003	0.013
84	Med	ACM, HVH, Pass, Level Turn Left - Aggress	0.000	0.001	0.002	0.008
86	Med	ACM, HVH, Pass, Level Turn Right - Modera	0.000	0.001	0.008	0.049
88	Med	ACM, HVH, Pass, Climbing Turn - 10- Pitch	0.000	0.018	0.017	0.111
89	Med	ACM, HVH, Pass, Climbing Turn - 20- Pitch	0.000	0.039	0.030	0.174
90	Med	ACM, HVH, Pass, Climbing Turn - 30- Pitch	0.000	0.015	0.015	0.084
91	Med	Pitch Back Attack	0.000	0.083	0.000	0.069
92	Med	ACM, HVH, Evasive Quick Stop	0.000	0.157	0.110	0.694
100	Med	HVH Free Engagements	0.000	0.083	0.000	0.069
110	Med	HVFW Free Engagements	0.000	0.083	0.000	0.069
112	Med	Low AOB Flight	0.000	3.887	1.647	6.411

5. LOADS VARIATIONS

The flight load time histories were recorded with high sampling rate during AH-1Z structural demonstration flights. The loads on the blade cuff are CF, torsion, Mx, and Mz. The flight loads are stored in a database with various options: maximum-minimum pair in each rotor revolutions, time history, maximum, and minimum in flight conditions. The loads stored in the database were analyzed by NAVAIR (Naval Air System Command) to obtain maximum Mx and Mz moments for each flight condition. The Loads provided to L-3 for analysis are displayed in Figures 9 and 10. The Mx and Mz moments are not in-phase. The ratio of Mx/Mz varies from maneuver to maneuver and is significantly different than the static test. For cuff PoF computation a single or multivariable load distribution is required. It is assumed that CF and torsion applied during the test do not vary significantly during fleet operational flight maneuvers. The variation in Mx and Mz were reduced to a single variable with the introduction of resultant moment concept, $Mr = \sqrt{M^2x+M^2z}$. The μ and σ, Normal distribution parameters were evaluated using a weighted average method. The weights were the number of cycles in each maneuver. The numbers of cycles are computed using percent time in the regime in usage spectrum, Table 2 and rotor rpm. It is assumed that for the complete percent of time i.e., for all rotor cycles within the regime the loads are the same.

The ή and β Weibull load distribution parameters were evaluated using the least square technique and maximum likelihood method, Table 3. The η values evaluated by

maximum likelihood method are higher than least square method, but β values are lower than the least square method indicating the lower slope and wider range of the Weibull distribution. The Weibull CPD of Mr displayed in Figure 11 is computed using Weibull parameters evaluated by least square method, but the Normal CPD of Mr exhibited in Figure 11 is calculated using parameters estimated by maximum likelihood method.

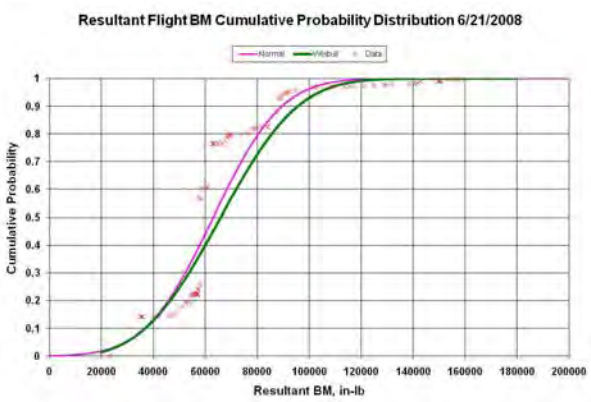

Figure 11: Resultant bending moment cumulative probability distribution

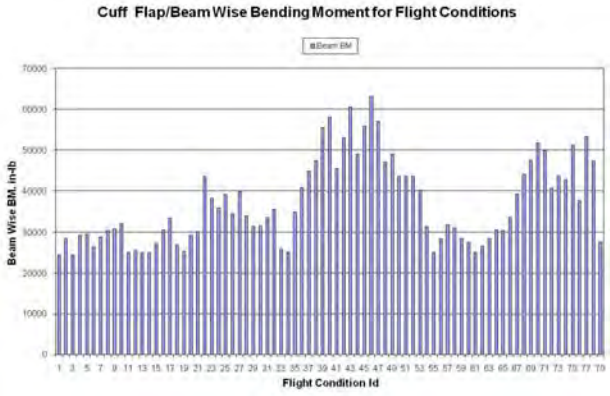

Figure 9: Cuff beam/flap wise bending moment for conditions in usage spectrum

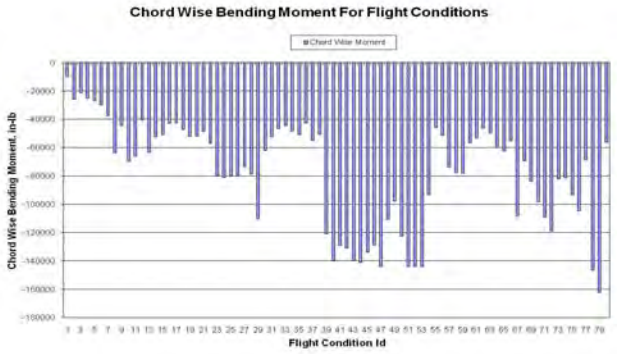

Figure 10: Cuff chord wise bending moment for conditions in usage spectrum

Table 3: Stress Weibull and Normal Distribution Parameters

	Stress Weibull Distribution						Stress Normal Distribution	
	Least Square Method			Maximum Likelihood Method			Maximum Likelihood Method	
	ή	β	r	ή	β		μ	σ
Mx	34303	4.664	0.954	41079	3.852		31601	5882
Mz	62380	2.630	0.872	89179	2.376		53992	21115
Mr	73865	3.232	0.852	98867	2.621		62974	20664

6. PROBABILITY OF FAILURE COMPUTATION

Whenever the Strength (S) is greater than the applied stress (s) the structure is reliable and PoF is zero. Thus, reliability (R) = P (S>s) = P(S-s>0), Reference 11. Figure 12 shows stress-strength inference areas of applied resultant moment/stress and resultant test moment/strength for Normal distribution. The reliability for normally distributed strength and stress is given by the following expression, Reference 11:

For reliability, strength should be greater than loads, (S-s) = y > 0

$R = P(y>0) = \int_{0}^{\infty} {}_{1}/ \sigma_y \sqrt{2\pi} \exp [-1/2 ((y - \mu_y)/ \sigma_y)^2] dy$

Probability of Failure (PoF) = 1-R

Where:

y = Strength, Mr. – Stress/Load, Mr.

$\mu_y = \mu_s - \mu_l$

$\sigma_y = \sqrt{(\sigma^2_S + \sigma^2_l)}$

μ_l = mean stress

μ_s = mean strength

σ_l = standard deviation load/stress

σ_s = standard deviation strength

Similarly Weibull distribution parameters of strength and stress indicated in Table 1 and Table 3 respectively were utilized to construct Weibull strength and stress CPD. The numerical approach outlined in Reference 11 was used to compute PoF.

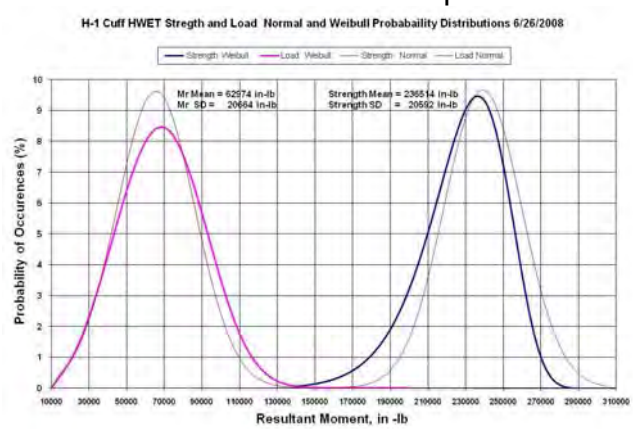

Figure 12: HWET strength and stress probability distribution

6.1. Normal and Weibull distribution PoF

The variation in the manufacturing process results in variation in the rotor blade cuff strength. Using the Normal distribution parameters of strength and stress, the PoF of a one hour flight is computed. The computed PoF is multiplied by four to account for the four cuffs in a rotor hub system. As the percentile strength decreases from 50 to 20 percentile, the PoF increases log linearly as shown in Figure 13. For strength variation from 50 to 2.3 percentile i.e., (μ to μ-2σ) the PoF increases from 5.41×10^{-11} to 1.141×10^{-7} in the case of Normal distribution, Table 4. As explained earlier, Weibull distribution fit to strength and stress have excellent correlation with finite lower and upper limits of the stress and strength distributions. Weibull distribution parameters of strength and stress were

utilized to compute PoF using interference theory. The PoF varies from $1.20x10^{-5}$ to $1.20x10^{-10}$ as strength increase from μ-3σ (0.1 percentile) to μ-1.5σ (6.7 percentile) as shown Figure 14. A five order of magnitude non linear variation. The Weibull distribution POF for μ-2σ strength is $8.33x10^{-9}$ compared $1.14x10^{-7}$ of Normal distribution indicating Weibull PoF one order of magnitude lower than Normal. Whereas for μ-3σ strength Weibull PoF significantly increases to $1.20x10^{-5}$ compared to $2.55x10^{-6}$ of Normal distribution revealing an increase in one order of magnitude. This behavior can be attributed to the shape of the tails of Normal and Weibull distributions. The prediction of PoF at the tails of distribution is difficult and uncertain. It is a function of probability distribution.

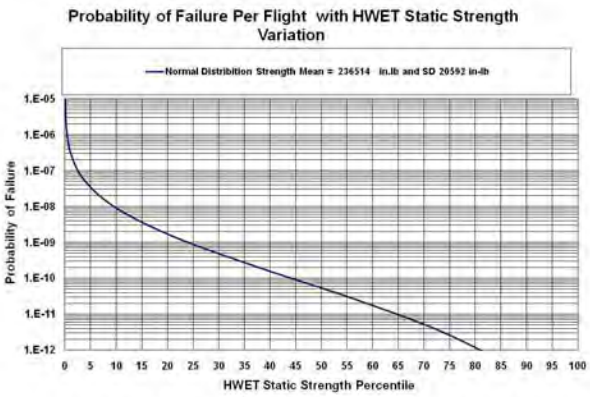

Figure13: PoF variation with percentile strength for Normal distribution

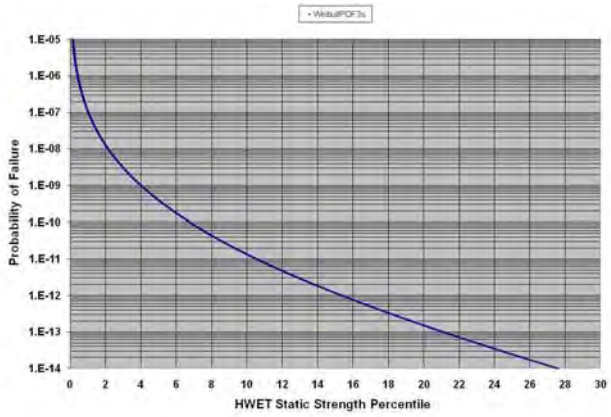

Figure 14: PoF variation with percentile strength for Weibull distribution.

Table 4: Probability of failures in a flight

	.		
Spectrum Type: μ+3σ			
Strength%		Normal	Weibull
50	μ	$5.41x10^{-11}$	$2.25x10^{-19}$
15.9	μ-1σ	$3.16x10^{-9}$	$7.89x10^{-13}$
6.7	μ-1.5σ	$2.02x10^{-8}$	$1.07x10^{-10}$
2.3	μ-2σ	$1.14x10^{-7}$	$8.33x10^{-9}$
0.1	μ-3σ	$2.55x10^{-6}$	$1.20x10^{-5}$

6.2. Effect of usage spectrum severity

The usage spectrum considered in previous computations was μ+3σ (worst case). However, most aircraft will fly an average usage spectrum with the number of rotor cycles shown in Figure 15. The occurrence of severe loads has been significantly reduced in comparison to μ+3σ spectrum as shown in Figure 8 and 15. This directly affects PoF as depicted in Figures 16 and 17. The PoF is decreased by two orders of magnitude for (μ-2σ) strength of Normal distribution and three orders of magnitude for a Weibull distribution, as shown in Tables 4 & 5. As strength percentile increases, the PoF difference between μ+3σ spectrum and average usage spectrum widens in the case of Normal distribution as well as Weibull. However, the difference in PoF from severe spectrum to average in the case of Weibull distribution is

of an order of magnitude of three, whereas for Normal distribution it is an order of magnitude of two.

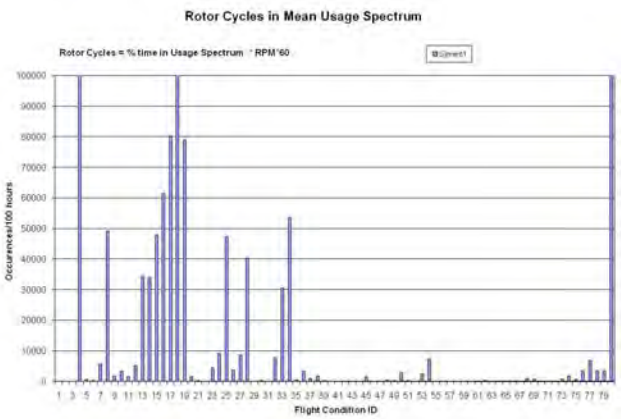

Figure 15: Rotor cycles for all flight condition in average usage spectrum.

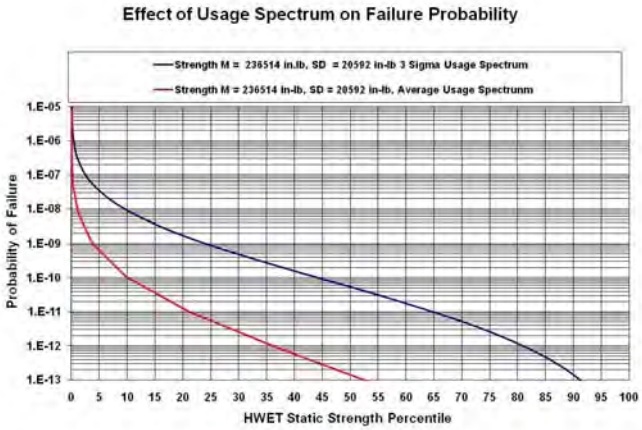

Figure 16: PoF for average and μ+3σ spectrum for Normal distribution.

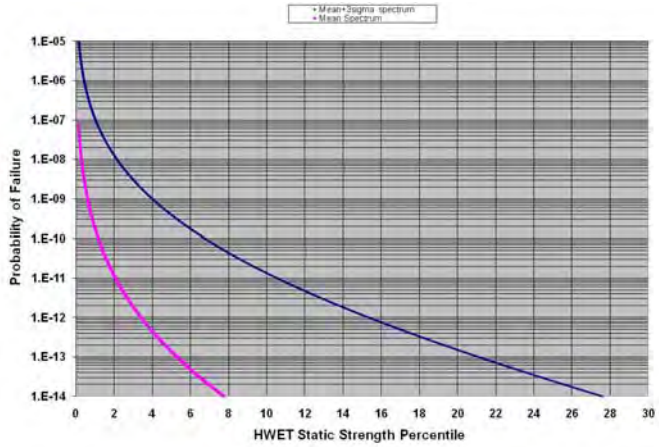

Figure 17: PoF for average and μ+3σ spectrum for Weibull distribution.

Table 5: Effect of Usage Spectrum on PoF

Spectrum Type: μ			
Strength%		Normal	Weibull
50	μ	1.42×10^{-13}	1.50×10^{-24}
15.9	μ-1σ	2.61×10^{-11}	4.82×10^{-17}
6.7	μ-1.5σ	2.82×10^{-10}	2.54×10^{-14}
2.3	μ-2σ	2.62×10^{-9}	6.64×10^{-12}
0.1	μ-3σ	1.44×10^{-7}	7.38×10^{-8}

6.3. Velocity envelope restriction

The restriction of dive from 185 to 165 knots results in the elimination of some high loads. This leads to the diminishing of PoF from 1.14×10^{-7} to 6.41×10^{-8} at μ-2σ strength as indicated in Figure 18 and Table 6**.** Thus, velocity restriction results in achieving greater safety. However, the decrease is not significant.

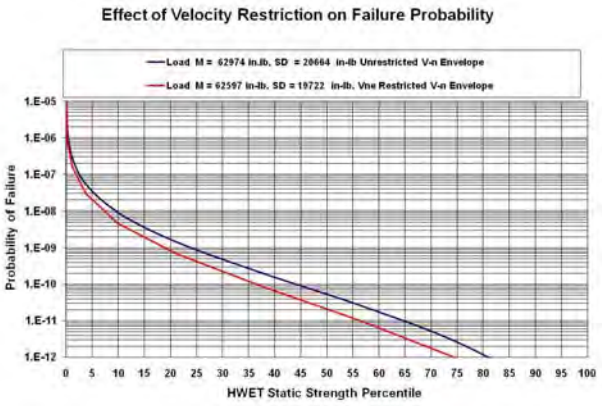

Figure 18: PoF for restricted velocity envelope.

Table 6: Effect of restriction on PoF

Normal Distribution		.	
Strength%		Unrestricted	Restricted
50	μ	$5.41x10^{-11}$	$2.13x10^{-11}$
15.9	μ-1σ	$3.16x10^{-9}$	$1.51x10^{-9}$
6.7	μ-1.5σ	$2.02x10^{-8}$	$1.05x10^{-8}$
2.3	μ-2σ	$1.14x10^{-7}$	$6.47x10^{-8}$
0.1	μ-3σ	$2.55x10^{-6}$	$1.68x10^{-6}$

6.4. Multivariable Distribution of Load and Strength

The measured Mx and Mz moments are shown in Figure 9-10. The cumulative probability distribution of these moments is created using the frequency of occurrence from the μ+3σ spectrum as shown in Figure 19. Furthermore, it is assumed that the magnitudes of these moments are independent of each other. However, the failure of the cuff is a function of Mx and Mz. Thus, stress acting on the cuff is the bivariate distribution of Mx and Mz. The Mx has Normal distribution with mean (μ_x) and standard deviation (σx) whereas Mz has Normal distribution with mean (μ_z) and standard deviation (σz). Therefore, bivariate Normal probability distribution has mean $\mu_j = \mu_x + \mu_z$ and standard deviation $\sigma_j = \sqrt{(\sigma^2_x + \sigma^2_z)}$. Similarly the bivariate Normal distribution parameters of strength were evaluated using the test data.

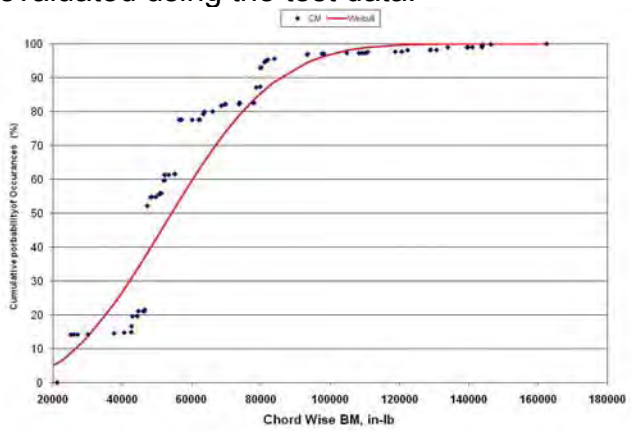

Figure 19a: Chord wise moment CPD.

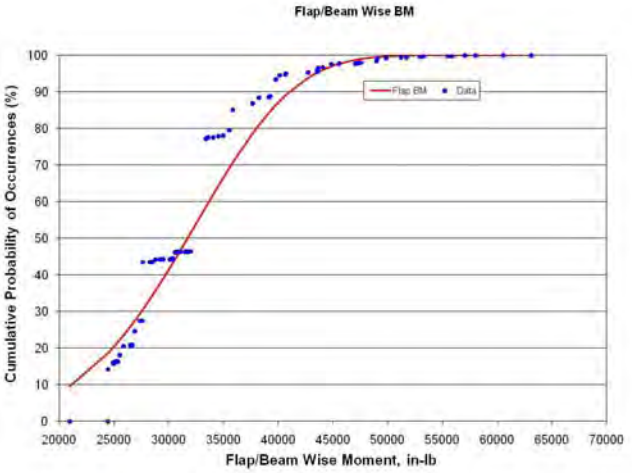

Figure 19b: Flap/Beam wise moment CPD

The interference theory was applied to compute PoF using the characteristics of strength and stress distribution. The comparison of PoF due to a single variable loading and multivariable loading is shown in Figure 20 and Table 7. Here it can be seen that under multivariable stress and strength distribution the PoF is lower than the single variable strength/stress at least by one order of magnitude. With the resultant loading, Mr has a lower standard deviation compared to multivariate loading distribution. Thus the failure risk predicted using resultant loading will be higher than multivariate loading. In reality each load type has a critical stress at

different points/locations on the structure, but this analysis provides the upper and lower bounds.

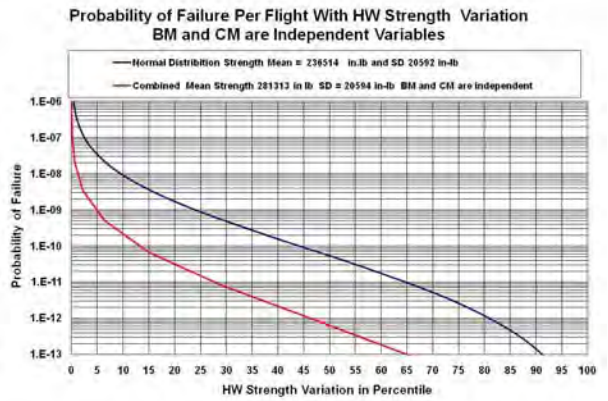

Figure 20: PoF for bivariate Normal distribution.

Table 7: PoF for Single and Multivariable Distribution

Normal Distribution			
Strength%		Single Varaible	Multivariable
50	μ	5.41×10^{-11}	6.46×10^{-13}
15.9	μ-1σ	3.16×10^{-9}	5.24×10^{-11}
6.7	μ-1.5σ	2.02×10^{-8}	3.98×10^{-10}
2.3	μ-2σ	1.14×10^{-7}	2.7×10^{-9}
0.1	μ-3σ	2.55×10^{-6}	8.86×10^{-8}

6.5. Multivariate Weibull distributions of load and strength

The various multivariable and bivariate Weibull distribution model are available in References 12-13. The complicated model form can be reduced to exponential form with a proper transformation. If Y_1 and Y_2 are two random variables, with transformation

$Z_1 = \lambda_1 Y^{\beta 1}$

$Z_2 = \lambda_2 Y^{\beta 2}$

The joint distribution of (Z_1, Z_2) is given by

$G(Z_1, Z_2) = 1\text{-}\exp\left[-(Z_1+Z_2)^{\alpha}\right]$

Where $\lambda_1 = (1/\acute{\eta}_1)^{\beta 1}$, $\lambda_2, = (1/\acute{\eta}_2)^{\beta 2}$, β_1, β_2 are parameters of marginal Weibull distribution and α an association parameter.

The association parameter α is assumed to be equal to 1 as the variation in flapping and chord moments/stress are independent. The bivariate probability density function is surface. The strength PDF surface shown in Figure 21 is evaluated by computing joint CPD for array of Mz for various values of Mx. From the CPD, the PDF is evaluated for various pair of (Mz, Mx). This process is repeated for stress PDF surface displayed in Figure 22. The intersection of strength and stress PDF surfaces will be failure surface. As example preliminary values of PoF at three strength pairs (Mz, Mx) are computed and indicated in Table 8. The PoF computed with bivariate is at least one order magnitude lower than univariate distribution. The detail PoF computation with intersection surface will be carried in next phase.

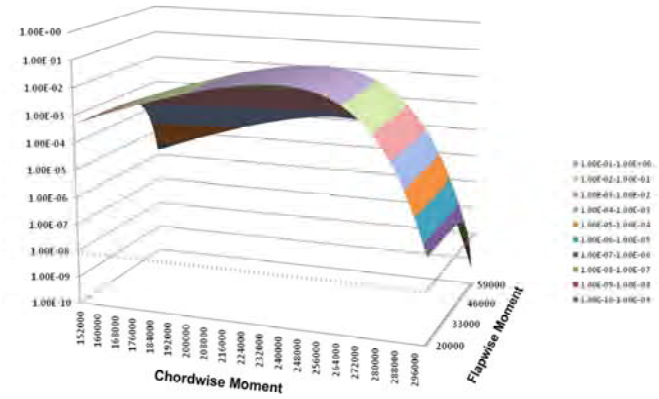

Figure 21: Strength bivariate Weibull probability distribution surface.

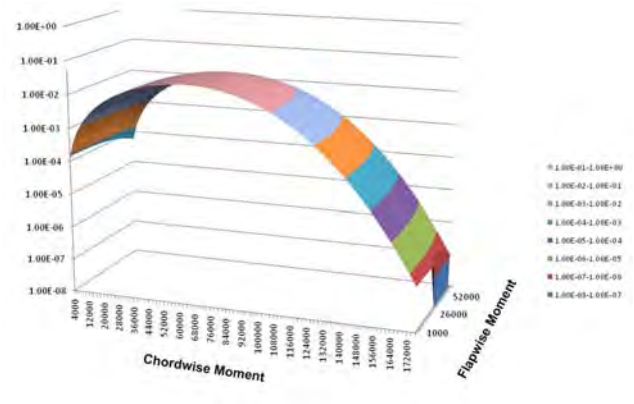

Figure 22: Stress bivariate Weibull probability distribution surface.

Table 8: PoF for Single and Multivariable Distribution

Weibull Distribution			
Strength%		Single Varaible	Multivariable
50	μ	$2.25x10^{-19}$	$2.06X10^{-15}$
15.9	μ-1σ	$7.89x10^{-13}$	$1.94X10^{-12}$
6.7	μ-1.5σ	$1.07x10^{-10}$	$2.33x10^{-12}$
2.3	μ-2σ	$8.33x10^{-9}$	$3.64X10^{-10}$

*Preliminary Analysis Values

6.6. Improvement in Bond Line Strength

The skin-stiffener debonding/delamination due to assumed defect and its location are discussed in Reference 14. Reference 14 also derives buckling load for an assumed defect and reveals that loads are reduced due to bending loading compared to an axial. Thus to avoid the cuff failure, it is necessary to improve inter-laminar strength. Recent advances in fiber matrix interface improvement with the addition of nanocomposite tubes and graphine nanocomposite tubes are promising technologies that are likely to help, References 15-16. However, the research is in its infancy. Its application in real word structures will take some time. It is difficult to detect debonding that occurs under loads in flight using (NDI) technique. However, the PZT embedded in structures holds promise as a structural monitoring technique, References 17.

7. CONCLUSIONS

1) The method has been developed to compute PoF variation with a percentile strength reduction for effective single variable loading and multiaxial variable loading environment.
2) The effect of usage severity on PoF has been investigated as expected the reduced severity decreases PoF.
3) The POF computed using effective single variable strength and stress distributions is higher that the multivariable strength and stress distribution.
4) The multiple failure distributions (Normal, Weibull, etc) shall be used to predict PoF as it is distribution dependent.

8. REFERENCES

1. Cassier, A. “Development of Triflex Rotor Head.” Journal of American Helicopter, Vol. 26, No.3 July 1981.
2. Huber, H. “Will Rotor Hubs Loose Their Bearings?” 18th European Rotorcraft Forum SP-506, 1992
3. Oldroyd, O., Sehgal A., Design Development, and Fabrication of the Model =, 430 Bearing less Main Rotor Yoke. AHS Forum 52, Washington, D.C. June 1996
4. Ajay, Sehgal “Design and Development of a four Bladed Bearingless Main Rotor System for the USMC H-1 Upgrade Program.” American Helicopter Society 55th Annual National Forum Proceedings, Montreal Quebec, Canada, May 25-27, 1999.
5. Gerhartz, J.J., Schopfel, A., and Huth, H., “Correlation Between Material Properties and Damage Tolerance Behavior of Composite Structures”, ICAF, 9-11 June 1993.
6. Weibull, W., “A Statistical Distribution Function of Wide Applicability,” ASME *Transactions-Journal of Applied Mechanics*, Vol. 18, 1951.
7 Barndt, G. and Moon, S., “Development of a Fatigue Tracking Program for Navy Rotary Wing Aircraft”, 50th Annual National Forum of the American Helicopter Society, Washington, D.C., May 1994.
8. Moon, S., Menon, D., and Barndt G., “Fatigue Life Reliability Based on Measured Usage, Flight Loads and Fatigue Strength Variations”, 52nd Annual National Forum of the American Helicopter Society, Washington, D.C., May 1996.
9. Moon S. and Phan, N., “Characterization of Rotorcraft Recorded Maneuver/Regime Usage Variability”, Sixth DSTO International Conference on Health and Usage Monitoring, Melbourne, Australia, 2009.
10. Moon, S., and Simmerman, C., “The Art of Helicopter Usage Spectrum Development”, The Journal of American Helicopter Society (AHS), Vol. 53, (1), January 2008, pp. 68-86 or AHS Forum 61, Grapevine, Texas June 1-3, 2005.
11. Kapoor, K.C. and Lambertson, L.R., “Reliability in Engineering Design, John Wiley and Sons, New York, 1977.
12. Lee, L., Multivariate distributions having Weibull properties, Journal of Multivariate Analysis 1979, pp 267-277
13. Lu, J.C. and Bhattacharyya, G.C., “Some New Construction of Bivariate Weibull Model Annals of the Institute of statistical Mathematics vol. 42.” 1990 pp 543-559.
14. Paris I.L., Krueger, R., O’Brien T.K., “Effect of Assumed Damage and Location on Delamination Onset for Skin-Stiffener Debonding, JAHS, October 2004.
15. S. L. Butler, A. Ghoshal, M. R. Gurvich, G. S. Welsh, M. R. Urban, and Bordick, “Analysis of Interlaminar Damages in Thick Rotorcraft Composite Components by Embedded Sensors" AHS Forum 66, May 2010, Phoenix AZ.
16. Y. Zhu, A. Sharma, C. E. Bakis, "Quasi-Static and Cyclic Interlaminar Cracking Behavior of Glass Fiber/MWCNT/Epoxy Hybrid Composites, AHS Forum 66, May 2010, Phoenix AZ.
17. M. A. Rafiee, N. Koratkar, "Graphene Nanocomposites-Potential for Rotorcraft Application” AHS Forum 66, May 2010, Phoenix AZ.